Mitchell McGaughy
Department of Mechanical Engineering,
Clemson University,
Clemson, SC 10028
e-mail: mmcgaug@g.clemson.edu

Chengshi Wang
Department of Mechanical Engineering,
Clemson University,
Clemson, SC 29631
e-mail: chengsw@clemson.edu

Eric Boessneck
Wind Turbine Drivetrain Facility,
Clemson University,
N. Charleston, SC 29405
e-mail: eboessn@clemson.edu

Thomas Salem
Wind Turbine Drivetrain Facility,
Clemson University,
N. Charleston, SC 29634
e-mail: tsalem@clemson.edu

John Wagner
Department of Mechanical Engineering,
Clemson University,
Clemson, SC 29631
e-mail: jwagner@clemson.edu

A Traveling Wave Thermoacoustic Engine—Design and Test

The demand for clean, sustainable, and cost-effective energy continues to increase due to global population growth and the corresponding use of consumer products. The provision of heat to a thermoacoustic prime mover results in the generation of an acoustic wave that can be converted into electrical power. Thermoacoustic devices offer highly reliable and transportable power generation with low environmental impact using a variety of fuel sources. This paper focuses on the design and testing of a single-stage, traveling-wave, thermoacoustic engine. The system configuration, component design, and integration of sensors will be described. Performance testing and system analysis show that for a 300 W heat source, the thermoacoustic machine generates a 54 Hz acoustic wave with a thermal efficiency of 7.8%. The system's acoustic power output may be increased by 84% through improved heat exchanger design. Tuning of the acoustic system and optimization of the bi-directional turbine merit attention to realize an applicable waste heat energy harvesting system. [DOI: 10.1115/1.4049528]

Keywords: acoustic power, heat exchangers, thermodynamics, thermoacoustic, energy management, energy/power systems, mechatronics

1 Introduction

The need for renewable and sustainable energy generation remains a challenge due to environmental concerns and increasing global electric demand. Solar and wind energy resources have been installed on both large and small scales throughout the world. However, some geographical locations lack sufficient sunlight and/or wind resources, leading to a need for alternative power sources. Thermoacoustic technology can utilize waste heat to produce acoustic power that can be further converted into electrical power. The required thermal energy can be supplied to a thermoacoustic prime mover by essentially any fuel source capable of generating high temperatures, including waste heat. Thermoacoustic systems are mechanically simple and, consequently, require minimal routine maintenance and/or lubrication. These systems are composed of a small number of components, so they can be readily transported and assembled. Thermoacoustic devices are environmentally friendly by design due to the use of air or inert noble gases as the working fluid.

Currently, two types of thermoacoustic systems exist: standing and traveling wave devices. Standing wave thermoacoustic devices were the first systems to intentionally convert thermal energy into acoustic energy at low efficiencies. Ceperley introduced the concept of using traveling waves to overcome the standing wave inefficiencies that are caused by necessary thermal delays and, consequently, inherit irreversibility [1]. The operation of this traveling wave thermoacoustic device is similar to the highly efficient and reversible Stirling thermodynamic cycle. In 1999, Backhaus and Swift developed an experimental thermoacoustic Stirling heat engine (TASHE) to overcome efficiency limiting losses within Ceperley's initial design [2]. The TASHE was constructed in a hybrid fashion with a traveling wave looped torus section attached to a standing wave resonator and operated at a record-setting 30% thermal efficiency. Recently, a pure traveling wave device was fabricated by De Blok which consisted of four core sections equally spaced within a looped feedback tube system [3]. These multi-stage traveling-wave thermoacoustic engines boast low operating temperatures due to low acoustic losses [4].

Traveling wave thermoacoustic devices are inherently reversible and therefore can operate as either a heat pump or prime mover dependent upon the component configuration. The core of a traveling wave thermoacoustic device consists of a high temperature (hot) heat exchanger and a low temperature (cold) heat exchanger to produce an axial temperature gradient in the regenerator. The acoustic wave within a thermoacoustic prime mover, or engine, is directed through a feedback piping network to be amplified by the regenerator. It is possible to install multiple core stages to improve system performance. An acoustic-to-electric conversion device can convert acoustic power into useable electric power.

A thermoacoustic prime mover, Fig. 1(*a*), accepts heat and produces an acoustic wave that propagates through the cold heat exchanger, into the regenerator, and out of the hot heat exchanger. In contrast, a thermoacoustic heat pump, Fig. 1(*b*), is supplied with an acoustic wave to pump heat from the cold heat exchanger into the hot heat exchanger for removal from the system.

This paper describes the design, assembly, and testing of a single-stage traveling-wave thermoacoustic engine with an examination of heat exchanger designs. This design is one of the first single-stage, traveling-wave, thermoacoustic engine to use a stub and turbine. The remainder of the article is organized as follows. In Sec. 2, mathematical concepts for the proposed thermoacoustic device are briefly introduced. Computer simulation results are presented in Sec. 3 to validate the design. In Sec. 4, the experimental system is explained followed by performance analysis concepts in Sec. 5. The experimental test results are presented in Sec. 6. Finally, the conclusion is contained in Sec. 7.

Manuscript received August 21, 2020; final manuscript received December 7, 2020; published online January 22, 2021. Assoc. Editor: Peiman Naseradinmousavi.

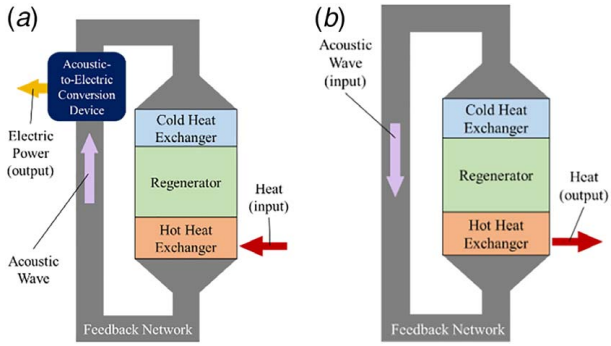

Fig. 1 Diagram of a conventional single stage traveling wave thermoacoustic system: (*a*) prime mover and (*b*) heat pump

2 Mathematical Concepts

Thermoacoustic interactions are applied to formulate an energy transfer realization of a compressible fluid, acted on by an acoustic wave, in contact with solid material. Rott derived the wave and energy equations for a single frequency acoustic wave propagating through a temperature gradient within a channel [5]. Ceperley found that a traveling acoustic wave propagating through a regenerator results in heat transfer characteristics similar to the Stirling cycle [1]. These thermoacoustic concepts may be applied to derive the mathematical equations that characterize the conversion within a traveling wave thermoacoustic engine.

In this project, a single-stage looped traveling-wave thermoacoustic engine was designed to convert input heat into acoustic power, as shown in Fig. 2. The experimental apparatus contains a thermoacoustic core featuring an ambient heat exchanger, regenerator, and hot heat exchanger. The core provides acoustic power amplification by executing a Stirling-like thermodynamic cycle, which converts heat into acoustic power [6]. The traveling acoustic wave provides compression of the working fluid and displacement toward the high-temperature section end of the core. The working fluid then expands and is displaced toward the low-temperature section of the core.

A gas parcel in the regenerator experiences thermal expansion as it is displaced toward the high-temperature region, and then thermal contraction as it is displaced toward the low-temperature region. The acoustic wave provides expansion and compression [6]. As mentioned before, the traveling-wave thermoacoustic device is reversible, and a heat pump can be generated by applying an acoustic wave in the opposite direction. The heat flow direction is always opposite to the direction of wave propagation in traveling-wave thermoacoustic devices.

An acoustic to electrical conversion devices, such as a bi-directional turbine or linear alternator, can be installed in the acoustic network to extract a portion of the acoustic power produced by the core. The excess acoustic power travels through the remaining feedback piping network and is directed back into the beginning of the core section to be re-amplified. An increase in acoustic volumetric velocity is produced by supplying acoustic power into a regenerator containing a steep temperature gradient in the direction of acoustic wave propagation [7]. The cross-sectional area of the core section can be increased relative to the feedback cross section to not only improve heat transfer effectiveness but also reduce viscous dissipation within the generator [8]. A thermal buffer tube (TBT) is attached to the bottom of the hot heat exchanger to thermally isolate the high temperate regions. A secondary cold heat exchanger is located at the TBT's end to remove radiative and conductive heat leaks down its wall in the absence of streaming effects [2].

Acoustic amplification by the core depends upon the absolute temperature ratio of the hot and cold ends of the regenerator or $\tau = T_h/T_c$. Figure 3 displays a lumped-element thermoacoustic engine model.

A network of channels consisting of varying compliance, inertance, and resistance is necessary to produce a near traveling-wave phasing within the regenerator [9]. The gas compressibility within a specified channel volume, or the compliance C, becomes

$$C = \frac{V}{\gamma p_m} \tag{1}$$

Similarly, the inertial properties of gas within the channel, or the inertance L, becomes

$$L = \frac{\rho_m \Delta x}{A} \tag{2}$$

The acoustic resistance is dependent on the oscillating acoustic wave velocity and pressure. Viscous, R_v, and thermal relaxation, R_k, resistances result from oscillating fluid velocity and pressure so that

$$R_v = \frac{\mu \pi \Delta x}{A^2 \delta_v}, \quad R_k = \frac{2\gamma p_m}{\omega(\gamma - 1) S \delta_k} \tag{3}$$

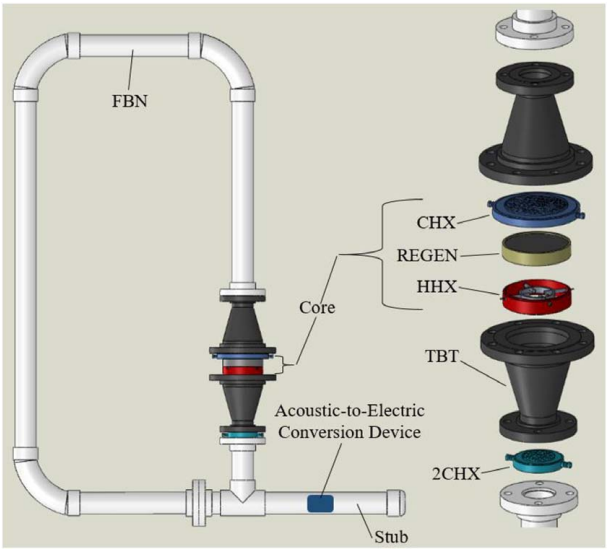

Fig. 2 Traveling wave thermoacoustic engine configuration

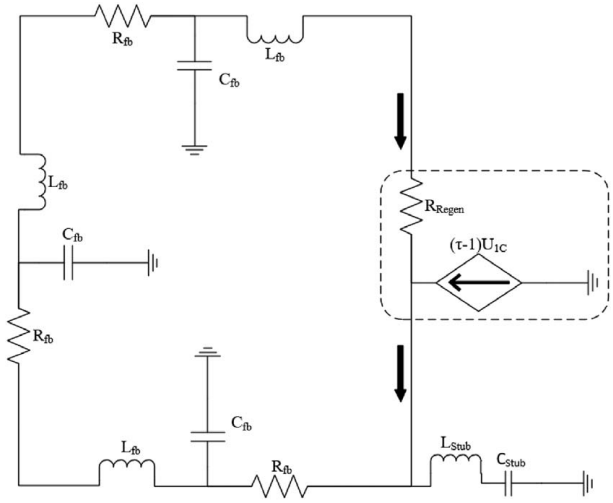

Fig. 3 Thermoacoustic engine lumped-element impedance model without an electric generator

These acoustic characteristics combine to form the acoustic impedance properties and are utilized in the formulation of the lumped element impedance model. The acoustic impedance, $Z=(p_1/U_1)$, is the ratio of pressure to volumetric velocity. A high impedance (e.g., high pressure and low volumetric velocity) is desired within the regenerator to avoid large viscous losses. The acoustic impedance can be expressed independent of channel geometry as the specific acoustic impedance, $z=AZ=(p_1/u_1)$. The characteristic acoustic impedance, $Z_0=(|p_1|/|u_1|)=a\rho_m$, is often used to quantify the medium for a generalized sound wave and is dependent on the properties of the medium. The form $|z|=Z_0$ denotes a lossless traveling wave, and $|z|\sim 20\rho_m a$ is the approximate desired condition within the regenerator of a traveling wave thermoacoustic engine [10].

The core (e.g., hot heat exchanger, regenerator, and cold heat exchanger) is represented as a resistance and volumetric velocity (current) source inside the dashed area of Fig. 3. Viscous losses produced in the regenerator are significant compared to the thermal-relaxation losses due to tight packing of mesh screens [7]. Furthermore, the axial change in temperature through the regenerator causes an inversely proportional change in density. As the conservation of the first-order mass flux must be upheld, $\rho_m U_1=$ constant, as temperature increases, the volumetric velocity must increase proportionally [2]. This volumetric velocity increase through the regenerator may be expressed as follows:

$$U_{1h}=\tau U_{1c} \tag{4}$$

The time-averaged acoustic power flow, $\dot{W}$, becomes

$$\dot{W}=\frac{\mathrm{Re}[p_1\widetilde{U_1}]}{2}=\frac{\mathrm{Re}[\widetilde{p_1}U_1]}{2} \tag{5}$$

where the tilde represents a complex conjugate. As the complex pressure amplitude at the hot and cold ends of the regenerator is approximately equal, the time-average power flowing out of the regenerator's hot end is dependent on the regenerator temperature ratio [2] or

$$\dot{W}_h=\tau\dot{W}_c \tag{6}$$

Therefore, the ratio of the temperature of the hot and cold end of the regenerator is a direct indication of acoustic amplification quantity. The reader is referred to Refs. [2,7] for more information on thermoacoustic system modeling.

Linear thermoacoustic theory, based on the linearization of the continuity, momentum, and energy equations, is applied to realize the relationship between pressure, velocity, and temperature to provide quantitative thermoacoustic estimations [7,11]. Rott's wave equation may be written as

$$[1+(\gamma-1)f_k]p_1+\frac{\gamma p_m}{\omega^2}\frac{d}{dx}\left(\frac{1-f_v}{\rho_m}\frac{dp_1}{dx}\right) \tag{7}$$

$$-\frac{a^2}{\omega^2}\frac{f_k-f_v}{1-\sigma}\frac{1}{T_m}\frac{dT_m}{dx}\frac{dp_1}{dx}=0$$

The relationship between the acoustic pressure, p_1, and the volumetric velocity, U_1, may be expressed by decoupling (7) into individual thermoacoustic momentum and continuity equations as

$$\frac{dp_1}{dx}=-\frac{i\omega\rho_m}{A(1-f_v)}U_1 \tag{8}$$

$$\frac{dU_1}{dx}=-\frac{i\omega A}{\gamma\rho_m}[1+(\gamma-1)f_k]p_1+\frac{(f_k-f_v)}{(1-f_v)(1-\sigma)}\frac{1}{T_m}\frac{dT_m}{dx}U_1 \tag{9}$$

The time-averaged acoustic power within a channel of length dx in complex notation becomes

$$\frac{d\dot{W}}{dx}=\frac{1}{2}\mathrm{Re}\left[\widetilde{U_1}\frac{dp_1}{dx}+\widetilde{p_1}\frac{dU_1}{dx}\right] \tag{10}$$

Let the viscous resistance per unit length, r_v, thermal-relaxation conductance per unit length, r_k, and complex gain/attenuation constant (dependent upon sign) for volume flowrate, g, be defined as follows:

$$r_v=\frac{\omega\rho_m}{A}\frac{Im[-f_v]}{|1-f_v|^2} \tag{11}$$

$$\frac{1}{r_k}=\frac{\gamma-1}{\gamma}\frac{\omega A}{\rho_m}Im[-f_k] \tag{12}$$

$$g=\frac{f_k-f_v}{(1-f_v)(1-\sigma)}\frac{1}{T_m}\frac{dT_m}{dx} \tag{13}$$

Equation (10) may be rewritten using Eqs. (11)–(13) as

$$\frac{d\dot{W}}{dx}=-\frac{r_v}{2}|U_1|^2-\frac{1}{2r_k}|p_1|^2+\frac{1}{2}\mathrm{Re}[g\widetilde{p_1}U_1] \tag{14}$$

The acoustic power is not directly affected by the inertance and/or compliance, but rather by viscous resistance, thermal-relaxation resistance, and thermally induced volume flowrate source/sink [11]. The viscous and thermal-relaxation dissipation terms always consume acoustic power. However, the gain/attenuation constant is dependent upon the magnitude and direction of the axial temperature gradient. Consequently, it may be considered to be a representation of the acoustic power produced or consumed [6]. These mathematical concepts explain the thermoacoustic phenomenon within the regenerator section of the thermoacoustic device.

3 Simulation-Based System Design

The thermoacoustic model provides a qualitative understanding of the alternative energy system. In addition, experimental testing and/or computer simulations may be employed to generate quantitative results. Experimental thermoacoustic systems can be constructed and optimized to improve performance. However, computer simulations are inexpensive and quick solutions for evaluating anticipated design changes. The Design Environment for Low-amplitude ThermoAcoustic Energy Conversion (DeltaEC) enables the design, troubleshooting, and improvement of these systems. This software utilizes linear thermoacoustic theory to numerically integrate a one-dimensional wave equation through user-defined segments and matches pressures, volumetric flowrates, and temperatures at junctions between segments [12]. Other variables and concepts, such as the energy equation, can also be implemented and analyzed within DeltaEC [13]. A series of estimate and target value pairs are required for the DeltaEC's shooting method, in which the initial values are gradually altered to successfully meet the specified targets.

A DeltaEC simulation was performed for the prototype single-stage traveling-wave thermoacoustic engine to provide an understanding of the various acoustic property distributions within the system. The simulations were compared to experimental findings to validate the approach. The DeltaEC model is composed of seven main segments as shown in Fig. 4. These segments include a cold heat exchanger (CHX), a regenerator (REGEN), a hot heat exchanger (HHX), a thermal buffer tube (TBT), a secondary cold heat exchanger (2CHX), a stub (STUB), and an acoustic feedback piping network (FBN). The total length of the combined elements with piping in the simulated system is 5.4 m.

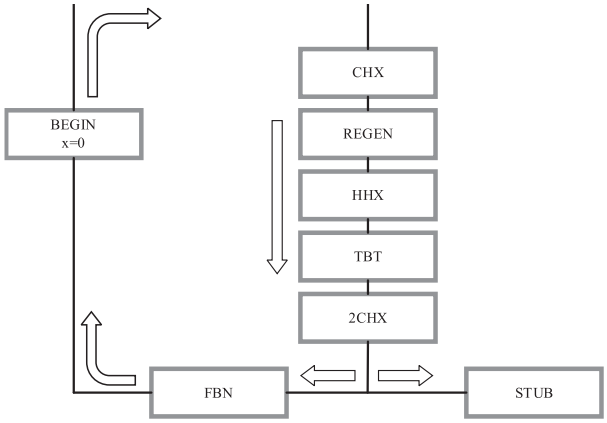

Fig. 4 Main components of the DeltaEC computer model and corresponding numerical integration path

Air at atmospheric mean pressure is specified as the working fluid to improve the construction and operation of the prototype. The system operates with a 54 Hz acoustic wave. The cold heat exchanger is modeled as a shell and tube heat exchanger in which the working fluid oscillates through the tubes. The hot heat exchanger is modeled as a parallel-plate heat exchanger. The regenerator is composed of a stack of mesh stainless steel screens and is modeled as such. The cross-sectional area of the thermoacoustic core (CHX, REG, HHX) is approximately two times greater than the feedback network cross-sectional area to reduce viscous losses in the regenerator by enforcing $|Z| \gg \rho_m a/A$ [3,8]. A high acoustic impedance in the regenerator is preferred for traveling wave conditions and leads to high pressure, low-velocity region which is desired to keep acoustic losses low [10]. This high acoustic impedance condition is produced by a large inherent flow resistance of the regenerator and generates a self-organization automation mechanism [10]. Additionally, a near traveling wave in the feedback network is desired to reduce dissipative effects [7]. The feedback network has a constant cross-sectional area.

The mathematical model was simulated for various input heat levels without an acoustic load. The regenerator and stub are located at 3 m and 3.6 m. Figure 5(*a*) displays the simulated pressure amplitude distribution through the thermoacoustic engine.

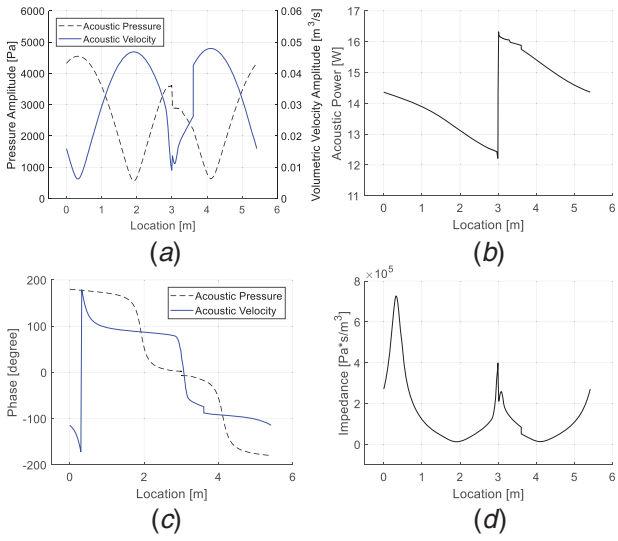

Fig. 5 Thermoacoustic engine numerical results: (*a*) acoustic pressure and volumetric velocity distribution, (*b*) acoustic power, (c) acoustic pressure and acoustic velocity phases, and (*d*) impedance

There are multiple locations of peak pressure amplitude. A steep negative pressure amplitude gradient is observed at the regenerator and results from the regenerator's high impedance. The standing wave ratio (SWR), comparing maximum and minimum pressure amplitude, is approximately 8.0. An SWR of unity represents an ideal traveling wave while a larger SWR (as observed in the simulation) reflects resonator acoustic losses [10]. The drive ratio (DR) compares the pressure amplitude to the mean pressure. A DR of nearly 4.5% exists at the location of maximum pressure amplitude. The stub does not cause a change in pressure amplitude magnitude but rather a modification in the rate of pressure amplitude change.

The simulated thermoacoustic engine volumetric velocity distribution is also shown in Fig. 5(*a*). Two minimums and maximums exist; one minimum is near the end of the cold heat exchanger just before the regenerator. Increasing the regenerator's cross-sectional area produces a decrease in the volumetric velocity. A sharp increase in the volumetric velocity amplitude is present at the regenerator and the stub. In the lumped impedance model, the regenerator has been modeled as a current source [7].

The acoustic power distribution through the system has been plotted in Fig. 5(*b*). Approximately 12.2 W of acoustic power enters the cold end of the regenerator and amplified to 16.3 W. The heat exchangers and feedback network each dissipate a small amount of the acoustic power. Figure 5(*c*) displays the acoustic pressure and volumetric velocity phase. In an ideal traveling wave, the pressure amplitude and volumetric velocity are in phase with each other. It is observed that the pressure and velocity phases are nearly in phase with each other at the regenerator location, which is desirable. However, the velocity and pressure amplitude are significantly out of phase in the feedback network which causes a high standing wave component and acoustic losses [10]. Lastly, Fig. 5(*d*) displays the acoustic impedance distribution. A high acoustic impedance, $18\rho_m a$, is observed at the regenerator which is close to the desired condition $20\rho_m a$. A steep drop in the impedance is noticed at the stub location due to an increase in compliance.

4 Experimental System

An 1.5 m × 3.0 m × 0.5 m experimental traveling-wave thermoacoustic engine was constructed. A larger cross-sectional area was selected for the core engine components to decrease the local velocity while keeping the mass flow constant. This action reduced the viscous losses in the regenerator and improved the heat transfer through the hot and cold heat exchangers. As expected, the component designs depend on the targeted performance characteristics [14] (refer to the Appendix for the component dimension details).

The primary cold heat exchanger, shown in Fig. 6(*a*), features a water jacket design. The working fluid oscillates through 901 parallel axial channels 3.175 mm in diameter; a porosity of 36.6% was realized. Clemson facilities water enters and exits the heat exchanger through barbed fittings to pass around the cylindrical block perimeter and reject excess heat.

The regenerator is composed of multiple randomly stacked stainless steel mesh screen disks. A laterally uniform temperature and linear axial temperature gradient are desired within the regenerator. The screens have a mesh number of 120 and a wire diameter of 66 μm. The porosity and hydraulic radius of the regenerator, ϕ and r_h, become

$$\phi = 1 - \frac{\pi n D_{wire}}{4} \tag{15}$$

$$r_h = D_{wire}\frac{\phi}{4(1-\phi)} \tag{16}$$

Therefore, the regenerator's porosity and hydraulic radii are approximately 75.5% and 50 μm. The hydraulic radius of the regenerator should be much smaller than the working fluid's thermal penetration depth to ensure good thermal contact between the solid material and working fluid.

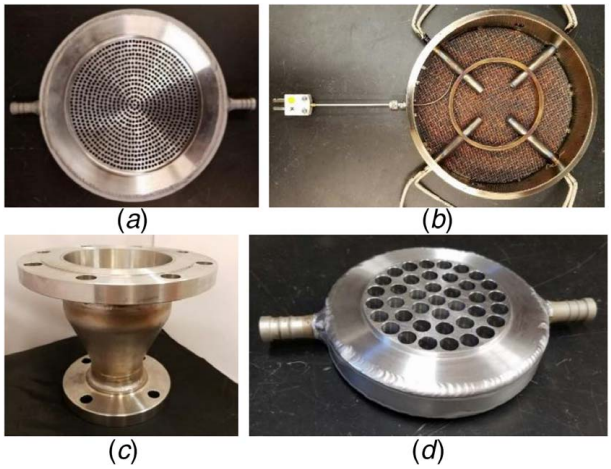

Fig. 6 Experimental thermoacoustic components: (*a*) cold heat exchanger, (*b*) hot heat exchanger, (c) concentric reducer/expander, and (*d*) secondary cold heat exchanger

The thermal penetration depth, δ_k, is a measure of the distance heat can be transferred laterally during acoustic oscillation. It depends on the working fluid properties and acoustic frequency so that

$$\delta_k = \sqrt{\frac{2k}{\omega \rho c_p}} \tag{17}$$

With atmospheric air pressure selected as the working fluid, the thermal penetration depth varies from approximately 360 μm to 700 μm through the regenerator. Therefore, the hydraulic radius of the mesh stainless steel screens is about seven times smaller than the smallest thermal penetration depth. The viscous penetration depth, δ_v, is a measure of the distance momentum can diffuse laterally during the acoustic oscillation and may be calculated as

$$\delta_v = \sqrt{\frac{2\mu}{\omega \rho}} \tag{18}$$

A smaller hydraulic radius improves thermal contact but also increases viscous losses through the regenerator. Consequentially, the design of the regenerator must be a compromise between good thermal contact and limited viscous losses [15].

A flattened expanded stainless steel disk with a thickness of 1.75 mm is located at the top and bottom of the regenerator to hold the stack of mesh screens in place. The expanded stainless steel disks rest on machined lips/edges, 3.175 mm thick, of the hot and cold heat exchangers which offer a small mixing region. Note that the heat rejected by the cold heat exchangers could not be measured due to instrumentation sensitivity limits.

The hot heat exchanger, refer to Fig. 6(*b*), is located below the regenerator and supplies the thermal power to the system. Heat is provided by four 120 VAC, 500 W heat cartridges. The heat cartridges are inserted into a small stainless steel ring located to improve stability and heat transfer to the working fluid. This heat exchanger contains four copper mesh screens with a mesh number of 22 and a wire diameter of 305 μm. The screens result in a porosity of 79.27% and hydraulic radius of 290 μm. They were intended to improve the distribution and transfer of heat and also act as flow straighteners to reduce jet-driven streaming within the thermal buffer tube. The hot heat exchanger is equipped with one K-type thermocouple to monitor the heat cartridge surface temperature to avoid overheating. The heat exchanger is capable of producing up to 2 kW of thermal power but the maximum heat input was limited by the cartridge's maximum operation temperature of 1033 K.

Two pipe reducer/expander assemblies, displayed in Fig. 6(*c*), are utilized above and below the thermoacoustic core section to provide gradual changes in cross-sectional diameter and avoid flow separation/transitional losses. Each concentric reducer/expander assembly consists of a pipe size 6 stainless steel flange, a pipe size 3 stainless steel flange, and a stainless steel concentric pipe reducer/expander. This component acts as a thermal buffer tube below the hot heat exchanger and is much longer than the peak-to-peak gas displacement amplitude to maintain thermal isolation. The TBT is recommended to be at least six times the peak-to-peak displacement of the working fluid [11]. The internal diameter of the thermal buffer tube is much larger than the thermal penetration depth and results in minimal heat transfer from the acoustic oscillation between the wall and gas [9].

A secondary cold heat exchanger, displayed in Fig. 6(*d*), is installed below the thermal buffer tube to maintain a near ambient temperature in the following feedback piping network. This component features a water jacket design, similar to the ambient heat exchanger above the regenerator. In the absence of performance degrading streaming, the secondary ambient heat exchanger will remove heat due to conduction through the thermal buffer tube walls, and radiative heat from the hot heat exchanger [2]. The secondary ambient heat exchanger contains 39, 9.5 mm diameter holes through which the working fluid oscillates; the porosity is 54%. The secondary heat exchanger is installed between the thermal buffer tube and feedback piping network to provide thermal isolation of the high-temperature region. Secondary cold heat exchangers are not required for the operation of thermoacoustic engines.

The feedback piping network is constructed of size 3, schedule 80, PVC piping, and pipe fittings. A stub is located approximately 289 mm from the bottom of the secondary cold heat exchanger. This stub provides additional volume that is necessary to lower the acoustic impedance to allow oscillations to begin [16]. A stub section is a required condition if a traveling wave thermoacoustic engine is configured with an odd number of thermoacoustic core sections [16].

Thermocouples and piezoelectric pressure transducers are utilized to monitor conditions and evaluate the performance of the experimental thermoacoustic apparatus. A steep temperature gradient through the regenerator is desired to maximize acoustic power. K-type thermocouples were inserted at the top and bottom of the regenerator and at the cross-sectional midpoint to monitor the regenerator's cold face and hot face temperatures. Piezoelectric pressure transducers monitor the acoustic pressure amplitude and analyze acoustic wave characteristics within the system. Multiple pressure sensor installation ports were installed at various locations in the feedback piping network.

A data acquisition system features bi-directional digital input/output (DIO), analog thermocouple input, and analog voltage input for monitoring and control. Current and voltage transducers measure the electric power delivered to the heat cartridges. A temperature controller maintains the specified surface temperature of the hot heat exchanger using a solid-state relay, thermocouple, and DIO channel. Figure 7 displays the 54 Hz single-stage traveling-wave thermoacoustic engine.

The assembled core section of the single-stage traveling-wave thermoacoustic engine is displayed in Fig. 8(*a*). A variable acoustic load, refer to Fig. 8(*b*), has been utilized to extract acoustic power from the feedback loop. It is constructed of a 1.03 L volume tank and globe valve. The valve setting controls the amount of acoustic power dissipated from the feedback piping network. The variable acoustic load can be considered as two lumped impedances, resistance and capacitance, in series since the dimensions are much smaller than the system's operational wavelength [17]. Two acoustic sensors are inserted; one at the inlet and another inside the tank. Since the acoustic load is considered as a lumped impedance, the pressure and phase are assumed to be constant throughout the entire tank [18]. The amount of

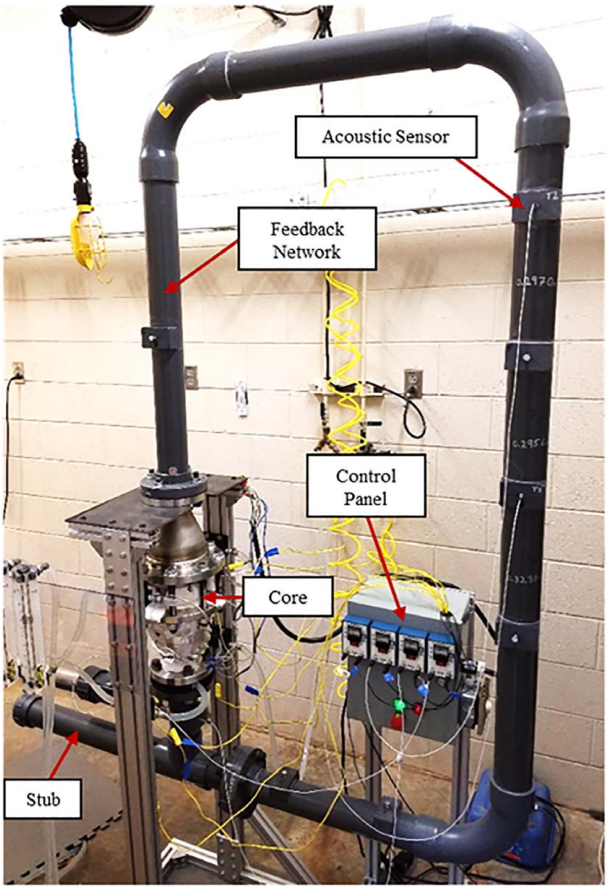

Fig. 7 Single-stage thermoacoustic engine

acoustic power dissipated by the variable acoustic load, W_{load}, may be expressed as

$$\dot{W}_{load} = \frac{\omega V |p_{inlet}||p_{tank}| \sin\theta}{2\gamma p_m} \tag{19}$$

where θ denotes the phase angle that p_{inlet} leads p_{tank}. The drive ratio of the engine can be controlled by adjusting the input heat and variable acoustic load. The variable acoustic load was limited to 1 W of acoustic power. The results presented in the remainder of this paper represent system operation with the variable acoustic load in the closed position (i.e., no dissipation).

A bi-directional turbine was placed in the stub to generate electricity from the acoustic power [19] The turbine converted the

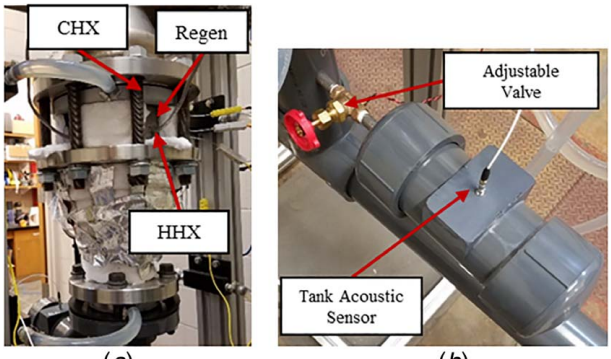

Fig. 8 Thermoacoustic engine: (*a*) core and (*b*) variable load

Fig. 9 Refined hot heat exchanger design

oscillating linear motion of the working fluid into rotational motion; the rotational direction is the same regardless of linear flow direction [20].

An alternative hot heat exchanger, shown in Fig. 9, was designed and installed into the thermoacoustic engine, to replace the preliminary hot heat exchanger and regenerator outer shell [21]. This new hot heat exchanger design allows system pressurization that will increase performance. Additionally, the hot heat exchanger is constructed of stainless steel and incorporates fins to improve heat transfer with the working fluid.

5 Performance Indicators

The acoustic power, along with other system characteristics such as temperatures and heat transfer, is primary indictors of thermoacoustic engine performance. The acoustic power within the feedback loop can be estimated from the acoustic pressure measurements and calculated via the two-microphone method. Two piezoelectric pressure sensors are installed at a distance much shorter than the wavelength apart from one another. The acoustic power flowing past the midpoint of the two pressure sensors, $\dot{W}$, is [11]

$$\dot{W} = \frac{A}{2\omega\rho_m \Delta x} |p_{1A}||p_{1B}| \sin\theta \tag{20}$$

A more accurate version of the two-microphone method accounts for attenuation in the laminar boundary-layer and does not require Δx to be much smaller than the wavelength [11] or

$$\dot{W} = \left(\frac{A}{2a\rho_m \sin(\beta)}\right) \tag{21}$$

$$\begin{pmatrix} Im[p_{1A}\widetilde{p_{1B}}]\left\{1 - \dfrac{\delta_v}{4r_h}\right. \\ \left.[1 - \Gamma + (1+\Gamma)\beta\cot(\beta)]\right\} \\ + \dfrac{\delta_v}{8r_h}(|p_{1A}|^2 - |p_{1B}|^2) \\ [1 - \Gamma + (1+\Gamma)\beta\csc(\beta)] \end{pmatrix}$$

where $\beta = (\omega\Delta x/a)$ and $\Gamma = \left((\gamma-1)/\sqrt{\sigma}\right)$.

The acoustic sensors installed in the thermoacoustic engine feedback piping network allow comparisons of the experimental and estimated pressure amplitudes. Figure 10 displays the DeltaEC

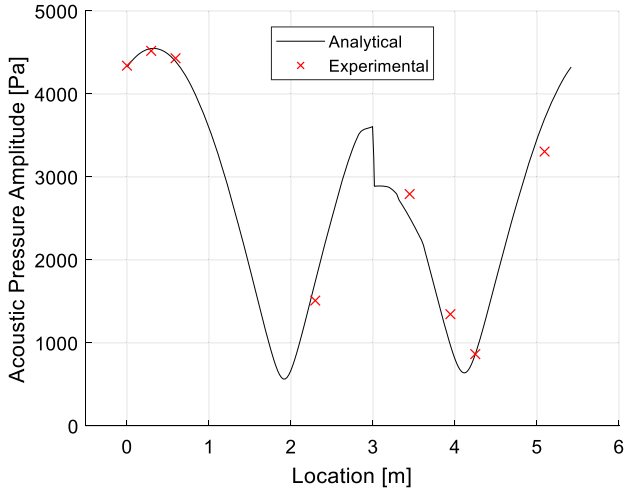

Fig. 10 Comparison of simulated and experimental acoustic pressure for thermoacoustic engine

pressure amplitude simulation versus experimental pressure measurements.

The temperature gradient across the regenerator and the heat applied to the system is analyzed to determine the efficiency of the engine. The thermal power applied to the system via the heat cartridges is $Q_h = \mathrm{IE}$. The heat extracted by the cold heat exchangers, Q_c, can be calculated as

$$Q_c = \rho c_p U(T_{out} - T_{in}) \tag{22}$$

The volumetric flowrate of ambient water through the main cold heat exchanger and secondary cold heat exchanger is measured. The water flow through each heat exchanger is 22.7 L per minute. However, the difference between T_{out} and T_{in} is smaller than the accuracy of the thermocouple. Therefore, the heat rejected by the cold heat exchangers was not analyzed in the final results.

The engine efficiency performance of the engine is determined from the heat applied to the system and the acoustic power created. The thermal to acoustic conversion efficiency, η,

$$\eta = \frac{\dot{W}}{\dot{Q}_h} \tag{23}$$

These power measurements should be performed once the engine has reached steady-state conditions [16]. The theoretical upper limit of the efficiency is determined by the Carnot efficiency, $\eta_C = (T_h - T_c)/T_h$. The engine efficiency with respect to the Carnot efficiency, $\eta_R = (\eta/\eta_C)$, becomes efficiency ratio.

6 Presentation and Discussion of Results

The pressure amplitude and acoustic power produced by the engine is dependent on heat supplied to the system. The maximum rated temperature of the cartridge heaters dictates the maximum heat input. The thermoacoustic engine was operated with four copper screens placed above the HHX heat cartridges, and also with them removed due to severe deterioration. The engine operation was conducted under input current ranges from 7.1 Amps to 11.41 Amps and the input heat ranges from 352.4 Watts to 923.9 Watts. The pressure amplitude, phase, and frequency have been recorded and used for acoustic power calculation. Then, the acoustic power combining with input heat forms the thermal to acoustic efficiency which serves as an index of the system's effectiveness. The acoustic power produced within the feedback network for various heat inputs without an external load is presented in Fig. 11(*a*); 32 W maximum acoustic power output was observed.

The engine with screens produced the greatest acoustic power. However, the thermoacoustic engine without screens produced

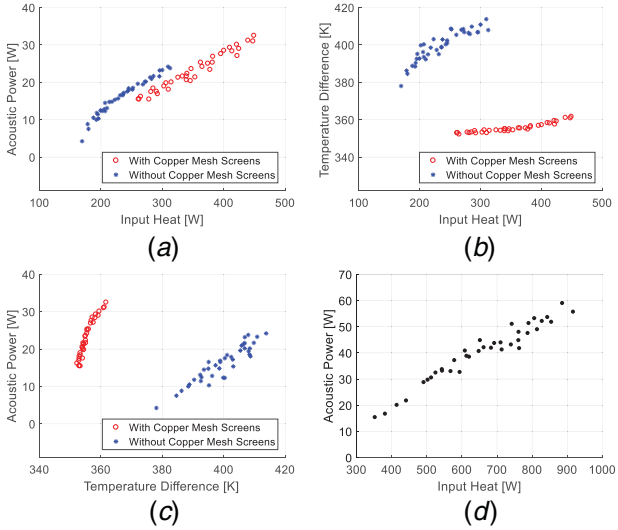

Fig. 11 Thermoacoustic engine operation: (*a*) acoustic power produced in feedback network, (*b*) temperature difference across the regenerator, (*c*) acoustic power versus temperature across regenerator produced in the feedback network, and (*d*) refined hot heat exchanger acoustic power output. The red circle denotes the data with copper mesh screens and blue asterisk represents the data without copper mesh screens.

Table 1 Measured thermoacoustic engine efficiencies

Configuration	η	η_C	η_R	$\dot{W}_{\max}$
Copper mesh screens	5.9–7.25%	53.6%	11–13.5%	32 W
Without copper mesh screens	4.2–7.8%	56.7%	9–14%	24 W
Alternative HHX	4.36–6.87%	64%	7.24–11%	59 W

greater acoustic power than the engine with screens for the same rated input heat and could operate at a lower amount. As per Fig. 11(*b*), the engine equipped with copper mesh screens produced a lower temperature difference across the regenerator at larger input heat ratings. As expected, a higher temperature difference is required for the engine without HHX copper screens (refer to Fig. 11(*c*)). A steep trend of acoustic power over a small temperature difference range indicates low acoustic losses [3].

As shown in Fig. 11(*d*), the refined hot heat exchanger design increases the acoustic power output of the system to a maximum of 59 W; An 84% improvement in comparison to the thermoacoustic engine with copper mesh screens. However, the resulting thermal to acoustic efficiency was reduced. This demonstrates an efficiency versus output power tradeoff for the new hot heat exchanger design.

The thermoacoustic engine configuration efficiencies are displayed in Table 1. Higher thermal efficiencies were produced for larger input heat levels with and without copper mesh screens. Acoustic effects are squared with increases in the drive ratio. However, loss mechanisms, such as heat, do not square with increases in the drive ratio. Hence, decreasing the importance of loss mechanisms at high-pressure amplitudes results in greater thermal efficiencies (to an undefined limit) [14]. The power generated by the turbine was minimal due to mechanical losses and not reported.

7 Conclusion

A single-stage thermoacoustic engine was designed, simulated, analyzed, and experimentally built. The simulation results, based

on the system mathematical model, closely match the test data. The thermoacoustic engine's maximum efficiency was 7.8%, corresponding to 14% of the Carnot efficiency. A maximum of 32.5 W of acoustic power was generated at the axial midpoint of the feedback network with the initial hot heat exchanger. After the implementation of the redesigned heat exchanger, the maximum efficiency decreased to 6.87% while the acoustic power output increased by 84%. The improvement of heat transfer to the working fluid at the location of the hot heat exchanger increases the acoustic power but the design changes reduced porosity, resulting in decreased efficiency. The heat exchanger design produces a dramatic effect on the output of the system. The bidirectional turbine that was placed in the stub to generate electricity from the acoustic power did not produce significant measurable power. Future activities may focus on the optimization of system components.

Acknowledgment

The authors would like to acknowledge the assistance of Kees de Blok[1] in the experimental design and construction of the thermoacoustic engine and Gregory Swift[2] for his technical support in modeling and simulating the thermoacoustic engine.

Conflict of Interest

There are no conflicts of interest.

Nomenclature

a = speed of sound (m s^{-1})
g = complex gain constant for volume flowrate
k = thermal conductivity (W m^{-1} K^{-1})
n = wire mesh number (m^{-1})
p = pressure (Pa)
u = velocity (m s^{-1})
x = position (m)
z = specific acoustic impedance (N s m^{-3})
A = area (m^2)
C = acoustic compliance (m^3 Pa^{-1})
E = electrical voltage (V)
I = electrical current (A)
L = inertance (kg m^{-4})
S = surface area (m^2)
U = volumetric velocity (K)
V = volume (m^3)
Z = acoustic impedance (Pa s m^{-3})
$\dot{W}$ = time-averaged acoustic power (W)
c_p = isobaric heat capacity per unit mass (J kg^{-1} K^{-1})
f_k = thermoacoustic spatially averaged viscous function
f_v = thermoacoustic spatially average thermal function
p_1 = complex pressure amplitude
p_m = mean pressure (Pa)
r_k^{-1} = thermal-relaxation conductance per unit length (m^4 Pa^{-1} s^{-1})
r_v = viscous resistance per unit length (Pa s m^{-4})
D_{wire} = mesh screen wire diameter (m)
Q_h = heat (W)
R_h = hydraulic radius (m)
R_k = thermal relaxation resistance (Pa s m^{-3})
R_v = viscous resistance (Pa s m^{-3})
T_c = temperature of regenerator cold face (K)
T_h = temperature of regenerator hot face (K)
T_{in} = inlet temperature (K)
T_m = mean temperature (K)
T_{out} = outlet temperature (K)
U_1 = complex volumetric velocity amplitude
U_{1c} = complex volumetric velocity amplitude at regenerator cold end
U_{1h} = complex volumetric velocity amplitude at regenerator hot end
$\dot{W}_c$ = time-averaged power flowing into regenerator cold end (W)
$\dot{W}_h$ = time-averaged power flowing out of regenerator hot end (W)
Im[] = imaginary component
Re[] = real component
Z_0 = characteristic acoustic impedance (N s m^{-3})
γ = specific heat ratio
Δ = difference
δ_k = thermal penetration depth (m)
δ_v = viscous penetration depth (m)
η = efficiency (%)
η_c = Carnot efficiency (%)
η_R = efficiency ratio (%)
λ = wavelength (m)
μ = dynamic viscosity (N s m^{-2})
ξ = gas displacement amplitude (m)
ρ = density (kg m^{-3})
ρ_m = mean density (kg m^{-3})
σ = Prandtl number
τ = temperature ratio
ϕ = porosity (%)
ω = angular frequency (rad s^{-1})
$\sim$ = complex conjugate

Appendix

Table 2 Dimensional characteristics of experimental system components

Component	Material	Cross-sectional diameter (mm)	Length (mm)
Primary CHX	Aluminum	155	22.2
Regenerator	Stainless steel	157.5	22.6
Heat cartridge	Incoloy sheath	9.5	63.5
HHX	Stainless steel	155	14.5
Concentric expander/TBT	Stainless steel	81–157	250
Second CHX	Aluminum	81	29
FBN	PVC Sch 80 piping	73	4800
Stub	PVC Sch 80 piping	73	686

References

[1] Ceperley, P. H., May 1979, "A Pistonless Stirling Engine–The Traveling Wave Heat Engine," J. Acoust. Soc. Am., **66**(5), pp. 1508–1513.
[2] Backhaus, S., and Swift, G. W., June 2000, "A Thermoacoustic-Stirling Heat Engine: Detailed Study," J. Acoust. Soc. Am., **107**(6), pp. 3148–3166.
[3] De Blok, K., 2010, "Novel 4-Stage Traveling Wave Thermoacoustic Power Generator," ASME 3rd Joint US-European Fluids Engineering Summer Meeting and 8th International Conference on Nanochannels, Microchannels, and Minichannels, Montreal, Canada, pp. 73–79.
[4] De Blok, K., 2012, "Multi-Stage Traveling Wave Thermoacoustics in Practice," 19th International Congress on Sound and Vibration, Vilnius, Lithuania.
[5] Rott, N., 1980, "Thermoacoustics," Adv. Appl. Mech., **20**, pp. 135–175.
[6] Yu, Z., and Jaworski, A. J., Feb. 2010, "Impact of Acoustic Impedance and Flow Resistance on the Power Output Capacity of the Regenerators in Travelling-Wave Thermoacoustic Engines," Energy Convers. Manage., **51**(2), pp. 350–359.
[7] Yu, Z., Jaworski, A. J., and Backhaus, S., Nov. 2012, "Travelling-Wave Thermoacoustic Electricity Generator Using an Ultra-Compliant Alternator for Utilization of Low-Grade Thermal Energy," Appl. Energy, **99**, pp. 135–145.
[8] De Blok, K., Dec. 2015, Private Communication.
[9] Telesz, M., 2006, "Design and Testing of a Thermoacoustic Power Converter," M.S. thesis, Department of Mechaniccal Engineering, Georgia Institute of Technology, Atlanta, GA.

[1]E-mail: c.m.deblok@aster-thermoacoustics.com
[2]E-mail: swift@lanl.gov

[10] Abduljalil, A. S. A., Yu, Z., and Jaworski, A. J., 2011, "Design and Experimental Validation of Looped-Tube Thermoacoustic Engine," J. Therm. Sci., **20**(5), pp. 423–429.
[11] Swift, G. W., 2002, *Thermoacoustics: A Unifying Perspective for Some Engines and Refrigerators*, Acoustical Society of America through the American Institute of Physics, Melville, NY.
[12] Ward, W. C., and Swift, G. W., June 1994, "Design Environment for Low-Amplitude Thermoacoustic Engines," J. Acoust. Soc. Am., **95**(6), pp. 3671–3672.
[13] Ward, B., Clark, J., and Swift, G., 2016, *Design Environment for Low-Amplitude Thermoacoustic Energy Conversion Version 6.4b2 User's Guide*, Los Alamos National Laboratory, Los Alamos, NM.
[14] Tijani, M. E. H., and Spoelstra, S., Nov. 2011, "A High Performance Thermoacoustic Engine," J. Appl. Phys., **110**(9), p. 093519.
[15] McGaughy, M., Boessneck, E., Salem, T., and Wagner, J., 2018, "Critical Design Elements for Traveling Wave Thermoacoustic Engines," Proceedings of the ASME 2018 Power and Energy Conference, 2018-7376, Lake Buena Vista, FL, June.
[16] Collard, S., 2012, "Design and Assembly of a Thermoacoustic Engine Prototype," B.S. thesis, Department of Environmental Engineering, Helsinki Metropolia University of Applied Sciences, Helsinki, Finland.
[17] Fusco, A. M., Ward, W. C., and Swift, G. W., Dec. 1991, "Two-Sensor Power Measurement in Lossy Ducts," J. Acoust. Soc. Am., **91**(4), pp. 2229–2235.
[18] De Block, K., Feb. 2017, Private Communication.
[19] De Blok, K., Owczarek, P., and Francois, M., 2014, "Bi-Directional Turbines for Converting Acoustic Wave Power Into Electricity," 9th PAMIR International Conference, Riga, Latvia, pp. 433–438.
[20] Kloprogge, T., 2012, "Turbine Design for Thermo-Acoustic Generator," B.S. thesis, Department of Aeronautical Engineering, Hogeschool INHolland, Delft, Neitherlands.
[21] Boessneck, E., and Salem, T., 2016, "Performance Characterization of Bi-Directional Turbines for Use in Thermoacoustic Generator Applications," Proceedings of the ASME 2016 Power and Energy Conference, ES2016-59372, Charlotte, NC.